Dynamical steering in an electron transfer surface reaction: Oriented NO(v = 3, 0.08 E i

Nils Bartels, Kai Golibrzuch, Christof Bartels, Li Chen, Daniel J. Auerbach, Alec M. Wodtke, and Tim Schäfer

Citation: The Journal of Chemical Physics **140**, 054710 (2014); doi: 10.1063/1.4863862
View online: http://dx.doi.org/10.1063/1.4863862
View Table of Contents: http://scitation.aip.org/content/aip/journal/jcp/140/5?ver=pdfcov
Published by the AIP Publishing

Dynamical steering in an electron transfer surface reaction: Oriented NO($v = 3$, $0.08 < E_i < 0.89$ eV) relaxation in collisions with a Au(111) surface

Nils Bartels,[1] Kai Golibrzuch,[1] Christof Bartels,[1] Li Chen,[2] Daniel J. Auerbach,[1,2] Alec M. Wodtke,[1,2] and Tim Schäfer[1,a)]

[1]*Institute of Physical Chemistry, Georg-August University of Göttingen, Tammannstraße 6, 37077 Göttingen, Germany*

[2]*Department of Dynamics at Surfaces, Max Planck Institute for Biophysical Chemistry, Am Faßberg 11, 37077 Göttingen, Germany*

(Received 8 November 2013; accepted 20 January 2014; published online 7 February 2014)

We report measurements of the incidence translational energy dependence of steric effects in collisions of NO($v = 3$) molecules with a Au(111) surface using a recently developed technique to orient beams of vibrationally excited NO molecules at incidence energies of translation between 0.08 and 0.89 eV. Incidence orientation dependent vibrational state distributions of scattered molecules are detected by means of resonance enhanced multiphoton ionization spectroscopy. Molecules oriented with the N-end towards the surface exhibit a higher vibrational relaxation probability than those oriented with the O-end towards the surface. This strong orientation dependence arises from the orientation dependence of the underlying electron transfer reaction responsible for the vibrational relaxation. At reduced incidence translational energy, we observe a reduced steric effect. This reflects dynamical steering and re-orientation of the NO molecule upon its approach to the surface. © *2014 AIP Publishing LLC*. [http://dx.doi.org/10.1063/1.4863862]

I. INTRODUCTION

Surface scattering experiments with beams of oriented molecules provide valuable insights into steric effects in surface chemical reactions.[1–6] Experiments with adsorbed molecules also reveal strong orientational influences, for example, surface aligned photochemistry.[7–9] This raises an important question: When oriented molecules approach a surface adsorption site, to what extent does the growing interaction with the surface re-orient the molecule either away from or towards a favorable reactive geometry? This re-orientation is often referred to as dynamical steering, a process which has been studied in detail for pure gas phase reactions.

An excellent example is the activated Cl + HD reaction, where van der Waals forces in the entrance valley play the key role in the reaction's dynamic.[10] Comparison of the experimentally measured branching ratio of the HCl and DCl products with the predictions of quantum mechanical calculations of reactive scattering demonstrate the decisive influence of van der Waals interaction. The slightly asymmetric minimum in the potential energy surface for a perpendicular approach of the Cl atom towards the HD molecule leads to a pronounced steering effect for reaction geometries with different angles. This drastically affects the branching ratio of the products HCl and DCl. When the Cl atom approaches the D atom first, the reaction yields predominately the DCl + H product, whereas in the opposite geometry—the Cl atom approaches the H atom first—the Cl atom is steered towards perpendicular geometries. See Fig. 3 of Ref. 10. Since the potential energy barrier is significantly higher for perpendicular reaction geometries, the Cl atom subsequently exits the entrance valley without reacting. Hence, the cross section for the HCl production is substantially lower than the for the DCl production. This result can only be reproduced in quantum mechanical calculations when van der Waals interactions in the entrance valley are taken into account.

In contrast, van der Waals interactions are much harder to investigate in surface dynamics due to the multi-dimensionality of systems typically studied. Nonetheless, steering phenomena have also been experimentally measured, for example, in the non-activated dissociative adsorption of H_2 on Pd(100). Here, the opposite effect than in the Cl + HD system is observed and the molecule-surface interaction steers the reactant towards geometries with enhanced reactivity. Thus, the dissociation probability increases when H_2 incidence energy of translation is reduced from 0.25 eV to 0.02 eV.[11] Six-dimensional quantum dynamical computations using a density functional theory (DFT) derived potential energy surface,[12,13] which reproduce a number of experimental observations, show H_2 can be re-orientated to a favorable reaction geometry at low incidence energy because the interaction time is large. At higher incidence translational energy, where the time for re-orientation is reduced, the reaction probability is also reduced.

The stereodynamics of reactions can be more complex if a reaction barrier is present. For activated dissociation of H_2 on the (111) surface of copper, steric effects are found to be strongly dependent on the H_2 molecule's vibrational, rotational, and translational energy.[14] Here, steric constraints are strong for reactive events that occur with little excess energy above the reaction barrier and relax with increasing translational energy. This, however, is strongly dependent on the H_2 molecule's internal excitation.

a)Authors to whom correspondence should be addressed. Electronic mail: tschaef4@gwdg.de

Recently, we have shown that electronically nonadiabatic vibrational relaxation of NO($v = 3$) occurring upon collisions at the (111) face of *fcc* gold is strongly orientation dependent.[15] Due to increased attraction when approaching the surface with the N-atom first, the NO molecules can approach the surface more closely than for configurations with the O-atom first. This results in more efficient electron transfer from the surface to the NO molecule—forming transient NO^-—an event which is essential to the electronically nonadiabatic vibrational relaxation.[16–22] Since this example of molecule-surface vibrational energy transfer involves electron transfer (ET) between NO and Au, this represents a rare opportunity to investigate the steric influences on an ET reaction at a surface. It should be further noted that the adiabatic relaxation channel plays at most a minor role in the vibrational relaxation mechanism of this system. This is mainly caused by the large frequency mismatch between the NO vibration and the phonons of the gold crystal.[22–25]

While computational methods have been dramatically improved and applied to problems in surface chemistry with great success, ET still represents a theoretical challenge. DFT, the most popular tool in computational surface chemistry, can fail to accurately describe ET.[26] Other challenges to DFT are weak forces like London-dispersion and hydrogen bonding interactions; these forces can strongly influence the orientation of a molecule in its approach to a metal solid surface. With this in mind, it is clear that the most advanced computational methods are needed to develop an accurate theoretical chemical description of the orientation dependence of electron transfer at solid metal interfaces. Measurements of the orientation dependence of reactions as a function of translational energy can provide a basis for developing and testing theoretical approaches.

In this paper, we extend our previous studies on the steric influences on ET surface chemistry over a wide range of translational incidence energies (0.08 eV $< E_i <$ 0.89 eV). We report surface-collision-induced, vibrational state-selective relaxation probabilities, and rotational state population distributions for initially oriented samples of NO. The steric effect is strong over nearly the entire range of incidence energies, but it decreases considerably for $E_i < 0.3$ eV. We attribute this decrease to the onset of dynamical steering at low incidence translational energies. These results represent a valuable benchmark for the development of improved theories of both ET and weak interactions between molecules and solid surfaces.

II. EXPERIMENTAL

A. Overview

Orientation experiments with the classical hexapole lens approach have severe problems to reach higher incidence energies than $E_i = 0.4$ eV due to the small dipole moment of NO,[27] the length of the hexapole needed becomes impractically long. To address this problem we developed a new method called *optical state selection with adiabatic orientation*, which is applicable at essentially any incidence energy and has been described in detail previously.[28] We now describe its implementation in this work.

Experiments are carried out in a Stark orientation molecular beam surface scattering apparatus displayed in Fig. 1. A pulsed supersonic molecular beam of rotationally cold NO molecules is produced by expanding mixtures (Table I) of NO seeded in different carrier gases into vacuum through a piezoelectric valve (1 mm diameter nozzle, 10 Hz repetition

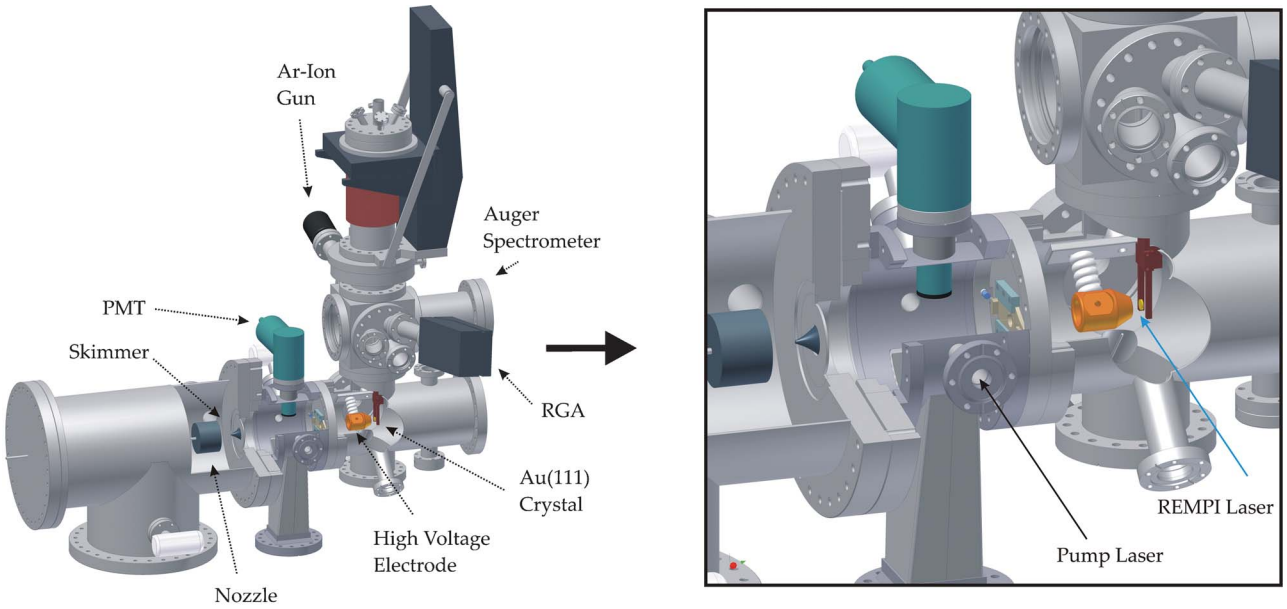

FIG. 1. Experimental setup of the orientation experiments. The molecular beam originates at the nozzle on the left side of the setup. The NO molecules in the molecular beam are vibrationally excited next to the photomultiplier tube (PMT), which is not used in these experiments. The high voltage electrode is mounted close to the surface enabling orientation of NO molecules due to the linear Stark effect. Ar-Ion gun, Auger spectrometer, and residual gas analyser (RGA) are used to ensure the cleanliness of the Au(111) surface. IR pump laser and UV resonance enhanced multiphoton ionization (REMPI) laser are shown as black and blue arrows, respectively.

TABLE I. Different NO/carrier gas mixtures employed for molecular beam surface scattering studies described in this paper.

Mixture	Translational energy
2% NO in H_2	0.89 eV
5% NO in H_2	0.68 eV
10% NO in H_2	0.48 eV
25% NO in H_2	0.27 eV
60% NO in Ar	0.08 eV

rate, 3 atm stagnation pressure). After passing a 2 mm electroformed skimmer (Ni Model 2, Beam Dynamics, Inc.) 3 cm downstream, the beam enters a differentially pumped region ($p \sim 10^{-8}$ Torr), where a part of the NO population is transferred into NO($v = 3$) by means of overtone pumping using a commercial narrow bandwidth pulsed IR Laser system, which is described in more detail in Ref. 29. Briefly, a single mode ring dye laser seeds a Nd:YAG pumped pulsed dye amplifier, which is used for difference frequency generation followed by optical parametric amplification (Sirah Lasertechnik). The system produces tunable IR light around 5544 cm^{-1} with >12 mJ pulse energy and 130 MHz linewidth. Depending on the desired final orientation, we excite either the high field seeking state or the low field seeking state of NO($v = 3$, $J = 0.5$) via the $X^2\Pi_{1/2}(v = 3) \leftarrow X^2\Pi_{1/2}(v = 0)$ $Q_{11}(0.5)_{e/f}$ transition. See Fig. 2.

The molecules then pass through a 2 mm aperture and enter the UHV chamber (base pressure $p = 10^{-10}$ Torr) where they are scattered from a Au(111) crystal. We calculate the number density at the maximum of the molecular beam pulse close to the surface to be $10^{11}/cm^3$. At these conditions gas-phase collisions with other molecules can be excluded.

A high voltage orientation electrode is mounted in front of the grounded gold crystal, where voltages between +15 kV and −15 kV can be applied. The electrode-crystal distance is 7 mm, yielding an electric field in front of the surface of up to 21.4 kV/cm. One μs after the NO molecules scatter from the surface, the voltage on the electrode is switched to ground potential unsing a high voltage switch (Behlke, HTS300). Results of vibrationally elastic and inelastic events are detected by means of (1+1)-REMPI (resonance enhanced multiphoton ionization) spectroscopy through the electronic $A^2\Sigma^+$ ($v = 0$) state employing the output of a commercial OPO laser system (Continuum Sunlite Ex, 3 GHz bandwidth, 2 mJ/pulse @ 255 nm) between 240 nm and 270 nm (4 mm diameter). The ions are accelerated onto a micro-channel plate detector (Tectra MCP 050 in chevron assembly) interfaced with an oscilloscope (LeCroy Waverunner LT344) for data collection. Before each experiment, the Au(111) crystal is cleaned by sputtering with an Ar-ion gun (LK Technologies NGI3000). The surface is then annealed for 20 min at 970 K and surface cleanliness is verified with Auger electron spectroscopy (Staib Instruments, Inc. ESA-150).

B. Production of oriented NO molecules

Orientation of NO molecules is achieved using *optical state selection with adiabatic orientation*. Its quantum mechanical treatment is described in detail in Ref. 28. The main principle is presented in Fig. 1 of Ref. 15.

First, a high resolution IR laser transfers population of the NO molecules into a pure quantum state of definite

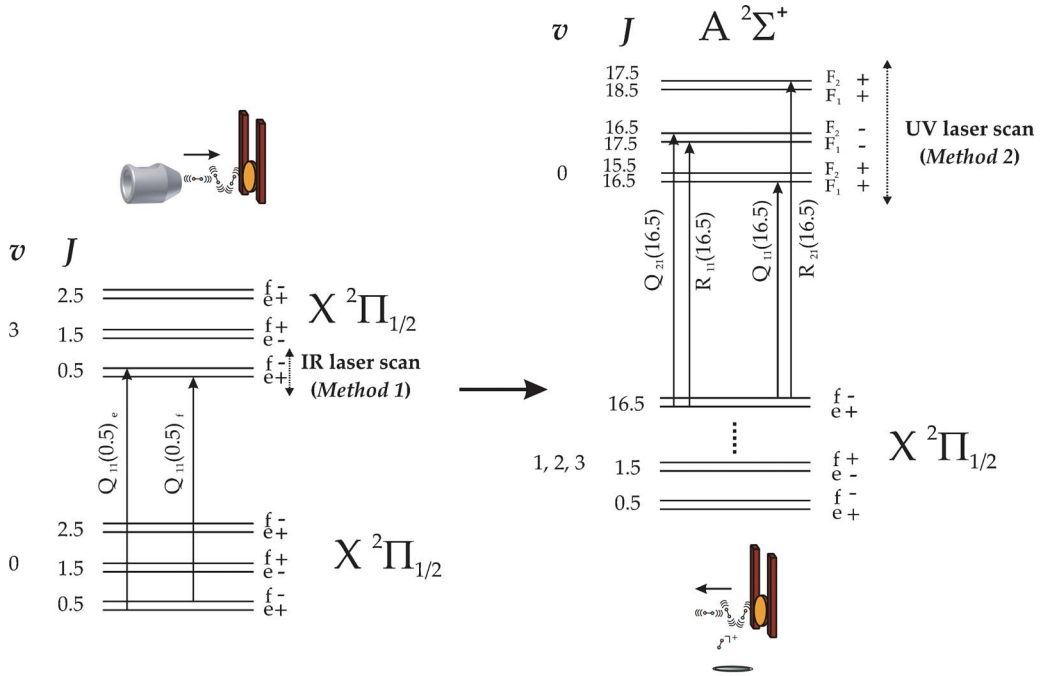

FIG. 2. Detailed Pump-Probe scheme of the performed experiment. In a first step, the IR laser excites either the low or high field seeking state in $v = 3$ via the $Q_{11}(0.5)_e$ or $Q_{11}(0.5)_f$ line, respectively. After scattering from the Au(111) surface, populations of NO molecules in $v = 3$, $v = 2$, or $v = 1$ are probed via the $A^2\Sigma^+(v = 0) \leftarrow X^2\Pi_\Omega(v = 3,2,1)$ bands, respectively. The dotted arrows illustrate the two different approaches described in the text. In method 1, the pump laser is scanned while the probe laser is fixed to detect a specific ro-vibrational line. This way, the asymmetry of that line can be measured directly. In method 2, the probe laser is scanned while the pump laser is fixed at either the low or high field seeking state, corresponding to two different orientations.

parity in NO($v = 3$, $J = 0.5$) (either e or f parity), which are split by approx. 0.01 cm^{-1} (Λ-splitting). The optically prepared molecules then fly into a region of strong electric field, and states are mixed by the Stark effect. Thereby, the prepared quantum states evolve adiabatically into oriented states with respect to the laboratory frame. The state, for which the potential energy increases in an electric field, is called low field seeking state, the other state is called high field seeking state. Switching the frequency of the IR overtone pump laser from the transition that populates the high field seeking state to the transition that populates the low field seeking state produces different orientations of the NO molecule in front of the surface and can be easily accomplished by tuning the IR light's frequency. Since the dipole moment of NO in $v = 3$ points from the partially negatively charged N-atom towards the partially positively charged O-atom, if the orientation electrode is biased negatively, the low field seeking state, which is energetically destabilized by the Stark interaction, evolves into an orientation hitting the surface with the O-atom first, whereas the high field seeking state, which is stabilized by the Stark interaction, evolves into an orientation with the N-atom pointing towards the surface. Of course, we can also change the NO orientation by reversing the electric field.

The uncertainty principle prevents perfect orientation, and orientation distributions calculated from the quantum mechanics of the NO molecule in an electric field for both high field seeking and low field seeking state for $X^2\Pi_{1/2}(v = 3, J = 0.5)$ are illustrated in Fig. 1 in Ref. 15. The average angle (expectation value $<\Theta>$) between electric field lines (which means surface normal for the employed experimental setup geometry) and dipole moment (bond axis) is 68° and 112°, respectively.

C. Two methods for probing the steric effect

Figure 2 shows the basic spectroscopy of the NO molecules needed to understand the experiment. As described in Sec. II B, the pump laser prepares NO($v = 3$) molecules in the incoming molecular beam with sufficient resolution to excite either the f- or the e-parity state of $J = 0.5$ (Fig. 2, left). After orientation by the electric field, molecules scatter from the Au(111) surface populating many rotational levels in $v = 3, 2, 1$, and 0. During the scattering process, the molecules lose memory of the initial parity. Except for $v = 0$, these population distributions are probed by REMPI spectroscopy via the $A^2\Sigma^+(v = 0)$ state (Fig. 2, right). Population in $v = 0$ produced by vibrational relaxation from $v = 3$ is invisible under the much larger population present in the molecular beam.

We use two approaches to probe the steric dependence of the scattering process, illustrated in Fig. 2: In method 1, we scan the IR-Pump laser back and forth over the range of the transitions producing f- and e-parity states and keep the UV-probe laser fixed at a REMPI transition probing one particular ro-vibrational level with $v = 3, 2$, or 1. In this way, the incident orientation of the molecule is "optically flipped." From the induced changes in the REMPI signal, one can directly compare the influence of incidence orientation on the final population of a specific state.

In method 2, we keep the IR-Pump laser fixed on one transition preparing one specific parity state (and thereby one orientation) while scanning the UV-Probe laser, recording an entire REMPI spectrum of surface scattered molecules. In principle, method 2 provides all necessary data. It suffers a practical disadvantage in that it requires excellent long-term stability in the entire Pump-Probe experiment.

III. RESULTS

A. Probing steric effects using method 1

Figure 3 shows illustrative outcomes of method 1 applied for probing the highly rotationally excited state NO($v = 3$, $J = 35.5$) produced in surface collisions with an incidence translational energy of $E_i = 0.89$ eV. The upper panel shows the REMPI signal as a function of the IR pump wavenumber for electric fields of 21.4 kV/cm (black solid line), 0 kV/cm (black dashed line) and −21.4 kV/cm (red solid line). For 0 kV/cm, the magnitude of the REMPI signal is independent

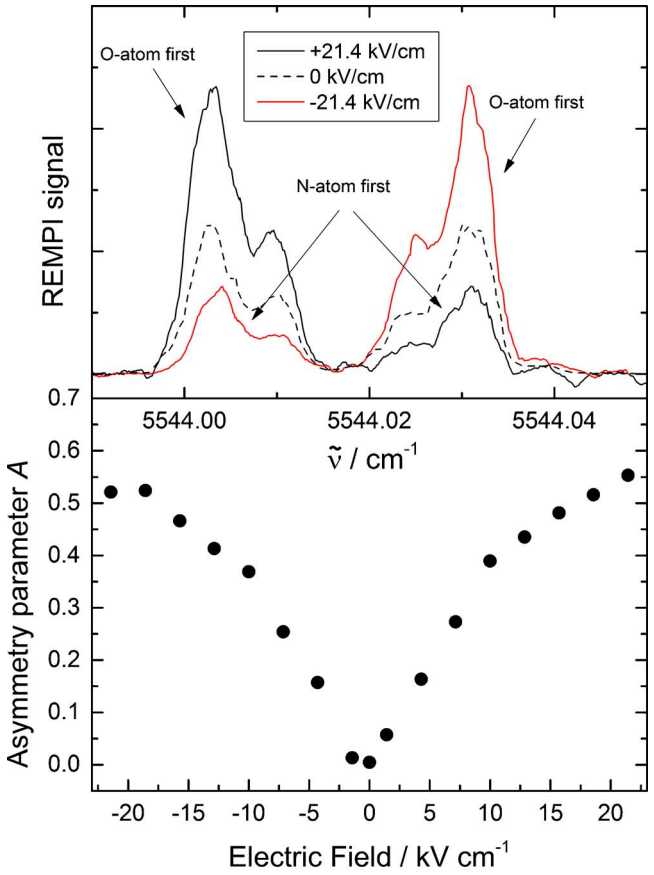

FIG. 3. (Upper panel) Detecting different scattering outcomes dependent upon molecular orientation (method 1 in the text). The two features in the IR overtone spectrum (Λ-doublets) correspond to two different orientations of the molecule prepared in the $X^2\Pi_{1/2}(v = 3, J = 0.5)$ state before it collides with the surface. The UV Probe laser is tuned to the $A^2\Sigma^+(v = 0) \leftarrow X^2\Pi$ ($v = 3$) $R_{11}(35.5)$ transition, providing selective detection of the $X^2\Pi_{1/2}(v = 3, J = 35.5)$ state produced by the NO collision with the Au(111) surface. Scattering to this state is strongly enhanced when NO approaches the surface with the O-atom first. (Lower panel) Dependence of the rotational line asymmetry on the electric field. The asymmetry parameter, $(I_O\text{-}I_N)/(I_O+I_N)$, is obtained by integrating the spectral features corresponding to O-first, I_O, and N-first, I_N, collisions, respectively.

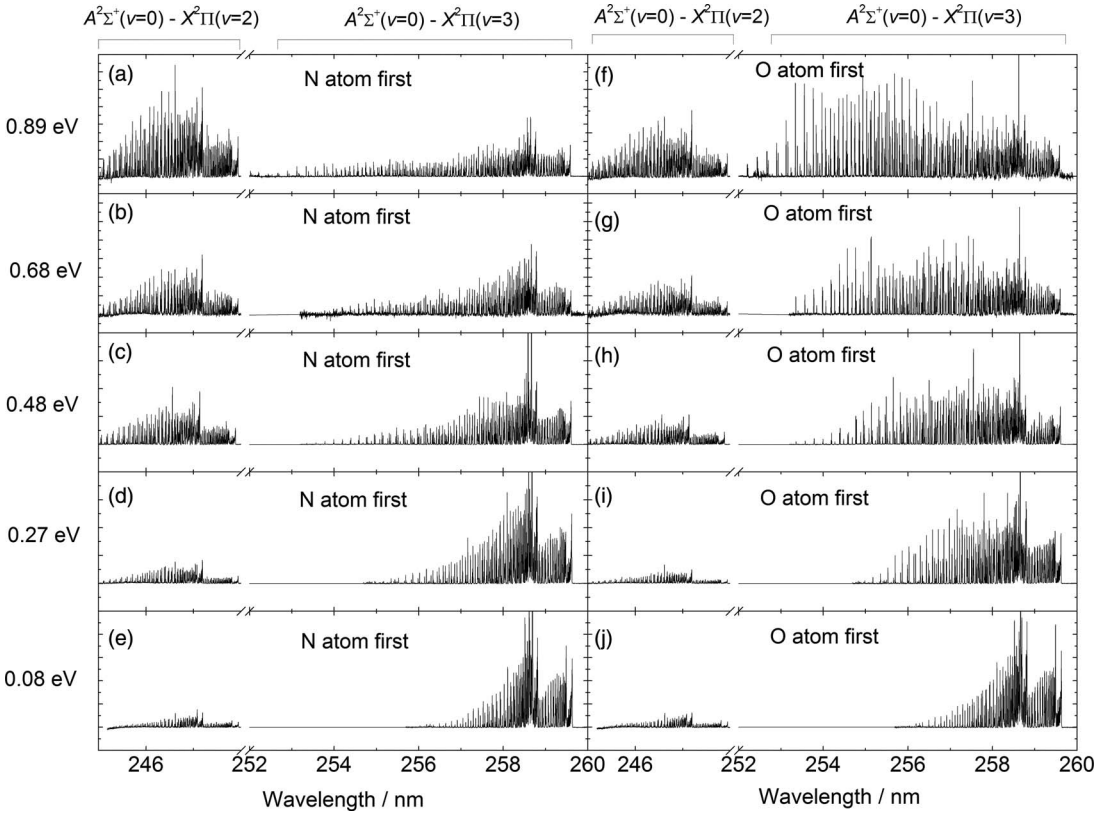

FIG. 4. (1+1) REMPI spectra of scattered NO($v = 3$) for five different translational energies in the spectral range between 240 nm and 260 nm for both orientations. Here, the IR laser is tuned to a transition that induces either N-first or O-first collisions (method 2). The UV laser scans over the $A^2\Sigma^+(v = 0)\leftarrow X^2\Pi_\Omega(v = 2)$ and $A^2\Sigma^+(v = 0)\leftarrow X^2\Pi_\Omega(v = 3)$ bands, which are well separated in the spectrum. One sees immediately both the effect of the incidence translational energy and the effect of the orientation on the REMPI spectra.

of which component of the Λ-doublet of the $v = 3$ state is optically prepared, reflecting isotropic orientation of the sample. This changes dramatically when the electric field is applied and oriented samples are produced. Here we find that REMPI signals produced from O-first collisions are much stronger than signals produced from N-first collisions. This means that this particular state NO($v = 3$, $J = 35.5$) is more strongly populated by O-first collisions than by N-first collisions.

We define an asymmetry parameter,

$$A = \frac{I_O - I_N}{I_O + I_N}. \quad (1)$$

Here, I_O and I_N are the REMPI signal intensities for collisions with O-atom and N-atom first, respectively. Figure 3 (lower panel) shows the derived asymmetry parameter as function of the electric field strength. It decreases monotonically from 0.53 to 0 between −21.4 kV/cm and 0 kV/cm and then increases again to 0.53 at +21.4 kV/cm. The flattening of the curve at high voltages is a sign that the quantum state specific maximum degree of orientation (68°, see Fig. 1 in Ref. 15) approaches saturation.

B. REMPI spectra from oriented scattering using method 2

More information can be extracted when scanning the REMPI laser over the whole ro-vibrational band and keeping the pump laser fixed on a specific transition producing one orientation (method 2). The resulting spectra for each orientation at five different incidence translational energies are shown in Fig. 4.

Both the $A^2\Sigma^+(v = 0)\leftarrow X^2\Pi_\Omega(v = 3)$ and the $A^2\Sigma^+(v = 0)\leftarrow X^2\Pi_\Omega(v = 2)$ bands are scanned between 245.5 nm and 260 nm and are well separated in the spectrum. Even a superficial visual inspection of the data reveals strong orientation effects. First, the ratio of the $A^2\Sigma^+(v = 0)\leftarrow X^2\Pi_\Omega(v = 2)$ band to the $A^2\Sigma^+(v = 0)\leftarrow X^2\Pi_\Omega(v = 3)$ band drops significantly when reducing the incidence energy, denoting a higher vibrational survival probability at lower incidence energies. Second, one observes enhanced intensities for the $A^2\Sigma^+(v = 0)\leftarrow X^2\Pi_\Omega(v = 2)$ band when scattering is performed with the N-atom first orientation. This effect corresponds to an increased NO($v = 3 \rightarrow 2$) relaxation probability for the N-first orientation. Furthermore, it is clear that this steric preference is less pronounced at lower incidence translational energies. Third, the rotational structure of the $A^2\Sigma^+(v = 0)\leftarrow X^2\Pi_\Omega(v = 3)$ band depends strongly on NO orientation, an effect that is not observed for the $A^2\Sigma^+(v = 0)\leftarrow X^2\Pi_\Omega(v = 2)$ band.

C. Analysis of ro-vibrational state distributions

From the spectra presented in Fig. 4, we extract rotational distributions from non-overlapping lines after correcting the peak areas for Hönl-London factors, intermediate state

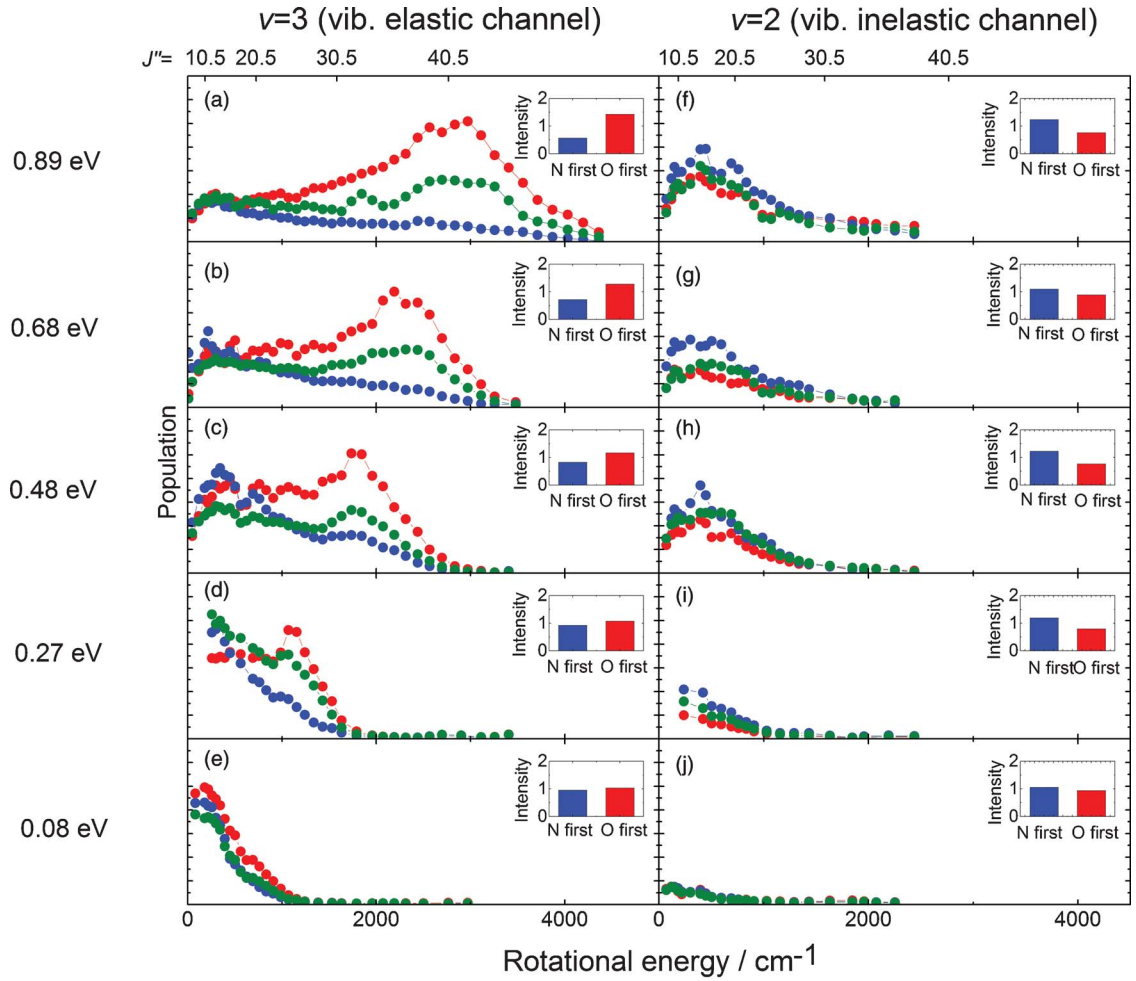

FIG. 5. Rotational state distributions for NO($v = 2$) and NO($v = 3$) for five different translational energies after scattering NO($v = 3$) from the Au(111) surface. The distributions have been deduced from the spectra presented in Fig. 4. The different colors denote N-first (blue), isotropic (green), and O-first (red) collisions. The rotational rainbow observed in the vibrationally elastic channel does not appear in the vibrationally inelastic channel. The insets show the integrated band intensities for both orientations and hence reflect the vibrational state survival probability and the vibrational relaxation probability to NO($v = 2$), respectively. The band intensities in the insets are scaled relative to the integrated band intensity of the isotropic signal.[31]

alignment, and partial saturation effects using the expressions of Jacobs and Zare.[30] The rotational distributions are plotted in Fig. 5 for each orientation, both vibrational states and all five different incidence translational energies.

Again, several features are important to note. We observe a clear rotational rainbow (peak at high J) for molecules scattered with the O-atom first in the vibrationally elastic channel (red curve in panels (a)-(e)). A similar rotational rainbow has been observed in scattering experiments of vibrationally ground state NO molecules from a Ag(111) surface.[1] In our work, we can clearly see that the rotational rainbow observed in the vibrationally elastic channel is strongly enhanced for O-atom first collisions, but still present for N-atom first orientation (blue curve in panels (a)-(e)). This shows that the rotational rainbow occurring for randomly oriented NO molecules (green curve) is dominated by O-atom first collisions. When decreasing the incidence energy of translation, the maximum of the rotational rainbow shifts towards lower rotational energies, until it essentially vanishes at the lowest measured incidence energy of 0.08 eV (panels (a)-(e)).

In contrast, no rotational rainbow is seen in the vibrationally inelastic channel depicted in panels (f)-(j), no matter what incidence translational energy or incidence orientation is used.

The insets in each panel of Fig. 5 show I_O and I_N (from Eq. (1)) integrated over all rotational states of $v = 3$ (left column) and $v = 2$ (right column). The integrated band intensities shown are relative values with respect to the integrated band intensity of the isotropic signal, which has been measured using another apparatus.[31] From the insets, we deduce the integrated band intensity ratios of NO($v = 3$) / NO($v = 2$) for the five different translational energies and both orientations. See Fig. 6. It clearly shows that the survival probability of NO($v = 3$) is significantly higher when scattering with the O-atom first and the influence of NO orientation on this survival probability decreases as the incidence energy of translation is reduced.

D. Rotational cooling upon vibrational energy relaxation

We next analyze the rotational excitation and its dependence on orientation and vibrational scattering channel. In Fig. 7, we plot the mean scattered rotational energy

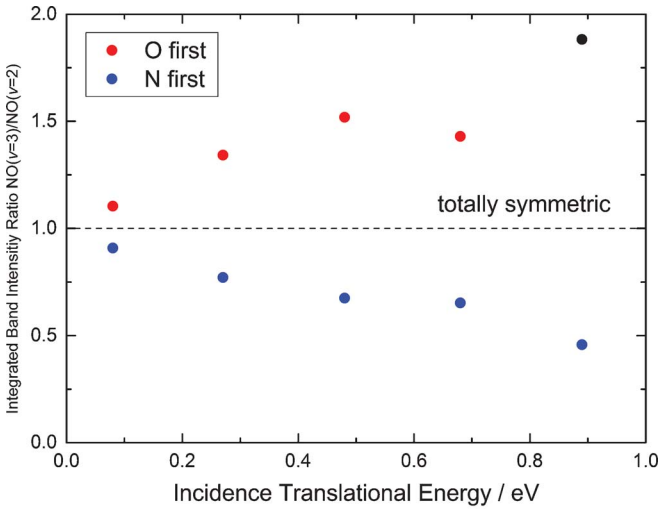

FIG. 6. Integrated band intensity ratio of NO($v = 3$)/NO($v = 2$) for five different translational energies and both orientations after scattering NO($v = 3$) from the Au(111) surface. The different colors denote N-first (blue) and O-first (red) collisions. The ratios are deduced from the insets in Fig. 5 and scaled relative to the integrated band intensity of the isotropic signal.[31] Thus, only the orientation effect is reflected, which clearly shows a decrease at lower incidence translational energies.

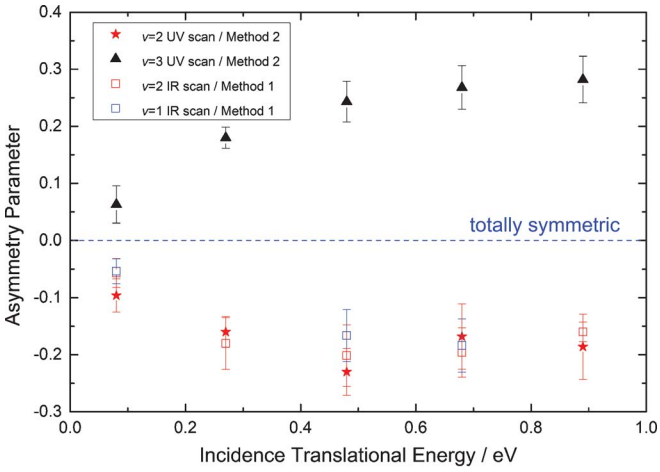

FIG. 8. Experimentally derived asymmetry parameters, $(I_O\text{-}I_N)/(I_O+I_N)$, for all of the vibrational scattering channels studied in this work as a function of the incidence translational energy. NO was prepared initially in $v = 3$ for all experiments and scattered from a Au(111) surface. Positive values of the asymmetry parameter denote an enhanced scattering population for O-atom first, while negative values represent enhanced population for N-atom first. The magnitudes of asymmetry parameters decrease towards zero as the incidence energy of translation is reduced. We attribute this to dynamical steering induced by weak reorienting forces experienced by the NO molecule on its approach to the surface.

$<E_{ROT}>$ versus the incidence translational energy. We find that $<E_{ROT}>$ exhibits a strong positive dependence on the incidence energy of translation for the vibrationally elastic channel ($v = 3 \rightarrow 3$). This effect occurs irrespective of the incidence orientation but is enhanced for O-first collisions. In contrast, $<E_{ROT}>$ values for the ($v = 3 \rightarrow 2$) channel are nearly independent of the incidence energy of translation or the incidence orientation. Furthermore, $<E_{ROT}>$ tends to be lower for the ($v = 3 \rightarrow 2$) compared to the ($v = 3 \rightarrow 3$) channel, except at the lowest incidence energies of translation.

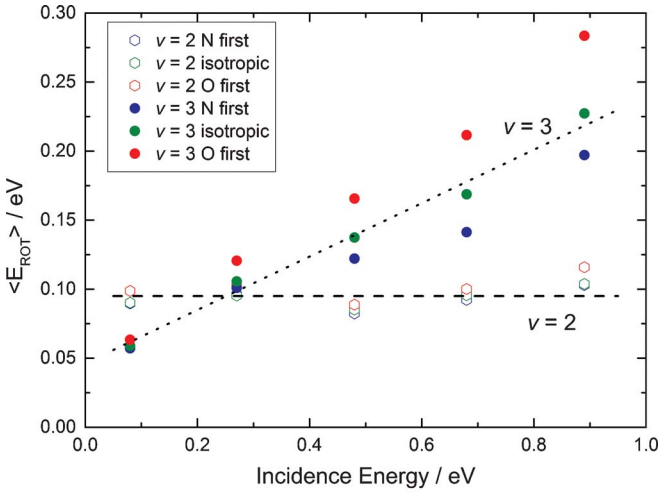

FIG. 7. Average rotational energy of scattered NO($v = 3$ and 2) molecules from Au(111) as function of the incidence translational energy and incidence orientation. Red color denotes O-first collisions, blue color denotes N-first collisions, and green color denotes isotropic scattering. The lines are shown to guide the eye and illustrate the different behaviour of elastically and inelastically scattered molecules.

E. Incidence energy of translation dependence of the steric effect

In Fig. 8, we present asymmetry parameters (Eq. (1)) for different vibrational channels and incidence translational energies. Black triangles and red stars (for $v = 3$ and $v = 2$, respectively) indicate asymmetry parameters derived from method 2 (Fig. 5, insets). Asymmetry parameters shown as red and blue open squares ($v = 2$ and $v = 1$, respectively) were determined employing method 1 where the UV-REMPI laser remains fixed at a specific transition and the IR-Pump laser is scanned over both orientations. For each point in the graph derived with method 1, we determined asymmetry parameters for several (~10) different rotational lines as described earlier and weighted the results according to the measured rotational state distributions of $v = 2$ as shown in Fig. 5. Asymmetry parameters in $v = 1$ are demanding to investigate using method 2 as the signal of the $v = 3 \rightarrow 1$ channel has to be measured on top of a large background arising from the scattering of thermally populated NO($v = 1$) in the molecular beam ($v = 1 \rightarrow 1$ channel).

In the probed range of incidence energies, scattering in the ($v = 3 \rightarrow 3$) channel exhibits asymmetry parameters greater than zero, reflecting the higher $v = 3$ survival probability for O-atom first collisions. In contrast, asymmetry parameters for the vibrationally inelastic channels ($v = 3 \rightarrow 2$) and ($v = 3 \rightarrow 1$) are negative, corresponding to the increased relaxation probability for N-atom first collisions.

The asymmetry parameters of $v = 2$ and $v = 1$, which are equal within experimental error, remain approximately constant over the range of 0.27 eV and 0.89 eV, but drop drastically at the lowest incidence energy of 0.08 eV. This important observation, which will be discussed later, is attributed to dynamical steering. The asymmetry parameter of

the ($v = 3 \rightarrow 3$) channel increases continuously with incidence energy of translation. This behaviour reflects the increased orientation dependent relaxation probability at higher incidence energies. Simply put, at higher incidence energies more N-first molecules are removed from the $v = 3$ state due to relaxation.

IV. DISCUSSION

The results presented in this work clearly show two characteristic features of the NO/Au(111) system. First, the vibrational relaxation probability of NO($v = 3$) molecules colliding with a Au(111) surface depends strongly on the incidence translational energy, the relaxation probability is significantly higher at elevated translational energies. Quantitative measurements on the relaxation probability have been carried out using another apparatus more suitable for quantitative measurements. The outcomes of this study have been recently published.[31]

Second, the results suggest a relaxation mechanism that strongly depends on the orientation of the colliding molecules: The survival probability of NO($v = 3$) is drastically reduced when the NO molecule hits the surface with the N-atom first. Signs for this orientation dependence have been found not only in theoretical studies but also indirectly in experimental work in the past, when rotational cooling associated with vibrational relaxation of non-oriented NO scattered from Au(111) was first discovered.[17]

The authors of Ref. 17 pointed out that their observations might result from either an orientation or site dependence of the electronically non-adiabatic coupling. They considered an orientation dependent effect the more likely explanation, but had no ability to distinguish the two possibilities as preparation of oriented NO molecules was not possible in that work.

Based upon the results presented in this work, it is now clear that the rotational cooling effect seen in that work is unambiguously due to an orientation dependence of the molecule-surface interaction. Our experimental outcome suggests that vibrational relaxation takes place only when the NO molecule approaches the surface within a certain angular range with the N-atom pointing towards the surface. All molecules outside of this angular orientation range are elastically scattered into $v = 3$. This interpretation can be deduced qualitatively from Fig. 5. Much more rotational excitation occurs when the NO molecules hit the surface with the O-atom first as can be seen from the red curves in Fig. 5(a)–5(e). On the other hand, the blue curves in Fig. 5(a)–5(e) show that the rotational excitation is suppressed when the NO molecule approaches the surface with the N-atom first. Hence, the shift of the rotational state distribution towards lower energies when the NO molecule is scattered inelastically to $v = 2$ (Fig. 5(f)–5(j)) can be explained by an angular filtering effect of the vibrational relaxation, since of course, only molecules, which underwent vibrational relaxation, are reflected in the rotational state distribution of $v = 2$. In other words, rotational cooling is a direct consequence of the vibrational relaxation's steric dependence. Due to the fact that vibrational relaxation predominantly takes place when the N-atom hits the surface first, the rotational excitation in the relaxation channel is governed by the attractive interaction of the N-atom with the Au(111) surface. This leads to significantly less rotational excitation than for the opposite repulsive orientation as can be observed in the vibrational elastic channel. We further found indication for a dynamical steering process that we observe at low translational incidence energies. Due to the forces the molecule experiences approaching the surface, the orientation induced by the comparably very weak Stark field is overcome and the molecule becomes steered to a configuration of large non-adiabatic coupling even when its initial orientation is unfavorable. This effect causes a decrease in the derived asymmetry parameters.[32]

Dynamical steering or re-orientation of NO in front of Au(111) has been predicted by first principles simulations employing the Independent Electron Surface Hopping (IESH) model. The reader is referred to Fig. 1 and Fig. 4 of Ref. 18. There, dynamical steering was deduced from the molecular orientation at the minimum distance to the surface of initially unoriented molecules. However, the steric effect is drastically diminished when simulating the here described experiments directly by using realistic orientation distributions of the incidence molecules derived from quantum mechanics.[33] The reader is also referred to Ref. 31, where the authors discuss the very detailed problems of IESH in the context of unoriented molecular beam surface scattering experiment of the same system (NO($v = 3$) scattered from Au(111)). *Indeed, we are presently aware of no theory capable of reproducing the observations of this paper.* This in all likelihood reflects weaknesses of DFT. So far, even the most sophisticated theories of electronically non-adiabatic molecule surface interactions like IESH require input data derived from DFT. Since DFT is known to suffer problems when applied to ET and is likewise challenged by weak steering forces that result from non-covalent interactions, new approaches to obtain *ab initio* electronic structure data for nonadiabatic models are needed if they are to successfully capture the observations of this work. One such method now being developed uses embedded correlated wave functions.[34–36] It would be interesting to use this method in combination with IESH in an attempt to improve the agreement of theory with experiment.

V. CONCLUSIONS

NO($v = 3$) molecules approaching the surface with the O-atom first exhibit a significantly higher survival probability compared to molecules hitting the surface with the N-atom first. Correspondingly, N-atom first orientations result in enhanced vibrational relaxation. At low incidence energies, the surface scattering appears to be governed by a dynamical steering process of the NO molecule, which orients the molecule into regions of strong non-adiabatic coupling in the vicinity of the surface. The fact that NO vibrational relaxation at Au(111) involves an electron transfer event as well as weak dynamical steering forces appearing only at incidence energies below 0.3 eV, make this an extraordinarily challenging benchmark for the development of modern theories of molecule surface dynamics and interactions. It is our hope that these results will inspire innovative new

theoretical approaches to the long standing problem of electronically non-adiabatic molecular interactions with solid metals.

ACKNOWLEDGMENTS

We would like to acknowledge support from the Alexander von Humboldt Foundation.

[1]F. H. Geuzebroek, A. E. Wiskerke, M. G. Tenner, A. W. Kleyn, S. Stolte, and A. Namiki, J. Phys. Chem. **95**, 8409–8421 (1991).
[2]M. Hashinokuchi, M. Okada, H. Ito, T. Kasai, K. Moritani, and Y. Teraoka, Phys. Rev. Lett. **100**, 256104 (2008).
[3]M. Okada, S. Goto, and T. Kasai, Phys. Rev. Lett. **95**, 176103 (2005).
[4]M. Okada, S. Goto, and T. Kasai, J. Phys. Chem. C **112**, 19612–19615 (2008).
[5]M. G. Tenner, F. H. Geuzebroek, E. W. Kuipers, A. E. Wiskerke, A. W. Kleyn, S. Stolte, and A. Namiki, Chem. Phys. Lett. **168**, 45–50 (1990).
[6]M. G. Tenner, E. W. Kuipers, A. W. Kleyn, and S. Stolte, J. Chem. Phys. **94**, 5197–5207 (1991).
[7]E. B. D. Bourdon, J. P. Cowin, I. Harrison, J. C. Polanyi, J. Segner, C. D. Stanners, and P. A. Young, J. Phys. Chem. **88**, 6100–6103 (1984).
[8]E. B. D. Bourdon, P. Das, I. Harrison, J. C. Polanyi, J. Segner, C. D. Stanners, R. J. Williams, and P. A. Young, Faraday Discuss. **82**, 343–358 (1986).
[9]J. C. Polanyi and R. J. Williams, J. Chem. Phys. **88**, 3363–3371 (1988).
[10]D. Skouteris, D. E. Manolopoulos, W. Bian, H.-J. Werner, L.-H. Lai, and K. Liu, Science **286**, 1713–1716 (1999).
[11]K. D. Rendulic, G. Anger, and A. Winkler, Surf. Sci. **208**, 404–424 (1989).
[12]A. Gross, S. Wilke, and M. Scheffler, Phys. Rev. Lett. **75**, 2718–2721 (1995).
[13]A. Gross and M. Scheffler, Phys. Rev. B **57**, 2493–2506 (1998).
[14]H. Hou, S. J. Gulding, C. T. Rettner, A. M. Wodtke, and D. J. Auerbach, Science **277**, 80–82 (1997).
[15]N. Bartels, K. Golibrzuch, C. Bartels, L. Chen, D. J. Auerbach, A. M. Wodtke, and T. Schäfer, Proc. Natl. Acad. Sci. U.S.A. **110**, 17738-43 (2013).
[16]J. W. Gadzuk, J. Chem. Phys. **79**, 6341–6348 (1983).
[17]A. M. Wodtke, H. Yuhui, and D. J. Auerbach, Chem. Phys. Lett. **414**, 138–142 (2005).
[18]N. Shenvi, S. Roy, and J. C. Tully, Science **326**, 829–832 (2009).
[19]N. Shenvi, S. Roy, and J. C. Tully, J. Chem. Phys. **130**, 174107 (2009).
[20]N. Shenvi, J. Chem. Phys. **130**, 124117 (2009).
[21]R. Cooper, C. Bartels, A. Kandratsenka, I. Rahinov, N. Shenvi, K. Golibrzuch, Z. Li, D. J. Auerbach, J. C. Tully, and A. M. Wodtke, Angew. Chem. **124**, 5038–5042 (2012).
[22]Y. Huang, C. T. Rettner, D. J. Auerbach, and A. M. Wodtke, Science **290**, 111–114 (2000).
[23]A. M. Wodtke, D. Matsiev, and D. J. Auerbach, Prog. Surf. Sci. **83**, 167–214 (2008).
[24]N. Shenvi, S. Roy, and J. C. Tully, J. Chem. Phys. **130**, 174107 (2009).
[25]A. M. Wodtke, Y. Huang, and D. J. Auerbach, J. Chem. Phys. **118**, 8033–8041 (2003).
[26]F. Libisch, C. Huang, P. Liao, M. Pavone, and E. A. Carter, Phys. Rev. Lett. **109**, 198303 (2012).
[27]M. G. Tenner, E. W. Kuipers, W. Y. Langhout, A. W. Kleyn, G. Nicolasen, and S. Stolte, Surf. Sci. **236**, 151–168 (1990).
[28]T. Schäfer, N. Bartels, N. Hocke, X. Yang, and A. M. Wodtke, Chem. Phys. Lett. **535**, 1–11 (2012).
[29]K. Golibrzuch, P. R. Shirhatti, J. Altschäffel, I. Rahinov, D. J. Auerbach, A. M. Wodtke and C. Bartels, J. Phys. Chem. A **117**, 8750–8760 (2013).
[30]D. C. Jacobs and R. N. Zare, J. Chem. Phys. **85**, 5457–5468 (1986).
[31]K. Golibrzuch, P. R. Shirhatti, I. Rahinov, A. Kandratsenka, D. J. Auerbach, A. M. Wodtke, and C. Bartels, J. Chem. Phys. **140**, 044701 (2014).
[32]Of course, a trapping/desorption mediated mechanism would lead to similar observations. But trapping/desorption is unimportant under our conditions. The trapping probability is small at the incidence energies used in this work and more importantly, trapped NO would emerge from the surface with a thermalized vibrational population distribution, and would (at our employed surface temperatures) not contribute to signals that probe $v = 1$ and 2.
[33]C. Bartels and S. Kandratsenka, private communication (2013).
[34]C. Huang and E. A. Carter, J. Chem. Phys. **135**, 194104 (2011).
[35]P. Huang and E. A. Carter, J. Chem. Phys. **125**, 084102 (2006).
[36]S. Sharifzadeh, P. Huang, and E. A. Carter, Chem. Phys. Lett. **470**, 347–352 (2009).